AIAA JOURNAL
Vol. 41, No. 8, August 2003

Airfoil Flow Visualization and Pressure Measurements in High-Reynolds-Number Transonic Flow

Herbert Olivier,* Thomas Reichel,† and Mitja Zechner‡
RWTH Aachen University, 52056 Aachen, Germany

Today most wind tunnels operated for aerodynamic testing are not able to reproduce flight Reynolds numbers. To overcome this problem, a shock tube flow is used to generate a high-Reynolds-number transonic flow. With this technique, Reynolds numbers up to 40×10^6 based on model chord length are attainable in the Mach number range between 0.6 and 0.9. Time-resolved surface pressure measurements, as well as flow visualizations, are performed for the airfoil BAC3-11/RES/30/21. Two models of different chord lengths, 80 and 100 mm, have been used. The maximum Reynolds number achieved to date is 38×10^6 for a freestream Mach number of 0.8. The results show that by calibrating the test-section flow carefully, this wind-tunnel technique can generate high-Reynolds-number flows, allowing aerodynamic testing at low cost. The technique avoids the complex cryogenic wind tunnel and model technique, at the expense of relatively short running times and relatively small test-section cross size. The testing time is on the order of 10–15 ms, which is sufficiently long for flow establishment and development of a useful measuring phase with stationary or at least quasi-stationary flow.

Introduction

MODERN civil transport aircraft cruise in the high transonic velocity region with flight Mach numbers in the range of 0.85 and Reynolds numbers based on wing chord length extending up to 50×10^6 or beyond. Wind-tunnel testing, still necessary for development, mostly suffer from low-Reynolds-number capabilities that make the extrapolation of wind-tunnel data to flight conditions difficult and/or questionable. Cryogenic wind tunnels have been developed to increase the Reynolds number to flight conditions. However, these facilities are extremely costly and require a complex wind-tunnel model and measuring techniques. Therefore, these facilities are not affordable, for example, for universities for the study of high-Reynolds-number transonic flows.

The idea to use the shock tube flow for aerodynamic testing is not new. Geiger et al.[1] described experiments performed in a shock tube to study transonic and supersonic flow patterns in 1949. Attempts to overcome the problem of relatively small test section sizes were made by area enlargement between driver and driven section[2] but at the cost of lower Reynolds numbers. In the past, a lot of work has been performed to study the influence of the test section walls on the model flow and how to minimize their effect.[3–8] This work showed that with suitable slotted test section walls in a shock tube it is possible to achieve the same flow as in a continuously working wind tunnel. More recently, this work was extended in Japan[9–12]; however, note that in all of these experiments the maximum Reynolds number based on model chord length did not exceed 2×10^6.

At the shock wave laboratory of RWTH Aachen University, a shock tube has been modified to perform airfoil testing at transonic Mach numbers and relatively high Reynolds numbers extending up to 38×10^6. The flow behind the incident shock wave provides the testing flow. Overall testing time is on the order of 10–15 ms, which is very short compared to that of conventional wind tunnels, but which is long enough for flow establishment and to perform reliable measurements during a stationary flow period.[13] The facility described offers the possibility to perform high-Reynolds-number testing at low cost and to avoid the cryogenic wind-tunnel technique, but at the expense of short running time and relatively small test-section cross size.

Presented as Paper 2002-0301 at the 40th Aerospace Sciences Meeting, Reno, NV, 14–17 January 2002; received 7 March 2002; revision received 11 February 2003; accepted for publication 4 April 2003.

*Head of Shock Wave Laboratory, Templergraben 55; olivier@swl.rwth-aachen.de. Member AIAA.
†Research Engineer, Shock Wave Laboratory, Templergraben 55. Member AIAA.
‡Research Engineer, Shock Wave Laboratory, Templergraben 55.

Description of the Facility

In Fig. 1 (top), the working principle of the tube is schematically shown. The shock tube is divided into a high-pressure and a low-pressure section by metal diaphragms. In this case, the high-pressure section is filled with compressed air up to an initial filling pressure p_4 at temperature T_4. The low-pressure section is filled with the test gas, typically nitrogen or air of pressure p_1 and temperature T_1. In our case, the temperatures T_1 and T_4 of the test and driver gas, respectively, match ambient temperature. Because of the pressure difference $p_4 - p_1$ after rupture of the main diaphragm, a planar shock wave develops that propagates with velocity u_s downstream into the low-pressure section compressing and accelerating the test gas at the same time. The strength of the incident wave is such that the desired transonic flow establishes behind it. Here, the main difference compared to the conventional wind-tunnel technique becomes obvious, where usually the desired flow condition is achieved by a nozzle expansion. In a shock tube, the flow is accelerated by the gasdynamic process taking place across a shock wave and, at the same time, is compressed to higher pressures and densities, offering the possibility to achieve a high-Reynolds-number flow. The total length of the shock tube used in this study is to 35.5 m, and its inner diameter is 300 mm. The maximum working pressure of the tube is limited to 25 MPa. The overall length of the facility consisting of shock tube, test section, and dump tank as shown in Fig. 1 (bottom) is 46 m.

Shortly after the bursting of the main diaphragm between the high- and low-pressure sections, the incident shock wave enters the test section, followed by the transonic flow. The test section is located at the downstream end of the low-pressure section. It consists of modular plates and forms a rectangular flow cross section. It is possible to install slotted or perforated inserts into the upper and lower wall to decrease wall interference effects. The inner cross section accommodating the model station has a fixed width of 0.2 m and a variable height of 0.2–0.28 m. Figure 2 shows a longitudinal view of the test section with a calibration rake installed at one of the two possible model positions. Entry and exit of the 2.2-m-long test section are formed as boundary-layer cookie cutters. These cookie cutters are designed as sharp-wedged leading edges of the upper

and lower walls, as well as of the side walls of the test section. The wedge with a wedge angle of 12 deg is located toward the bypass channel, whereas there is a plane surface oriented toward the inner part of the test section (Fig. 2). The test flow that is generated in the circular shock tube enters the rectangular test section, where the sharp edges of the cookie cutters cut out a homogeneous core flow and divert most of the shock tube boundary layer into separate bypasses around the test section. In this way during the quasi-stationary measuring phase, for the test section an almost fresh wall boundary layer develops with a running length for the upstream test position of only 556 mm and for the downstream position of 1300 mm. This holds for the nearest position of 200 mm of the upper and lower test section wall, respectively. The boundary-layer thickness of the shock tube flow at the test section has been estimated according to the theory of Mirels.[14] It grows from 0 up to 60 mm within 20 ms. This holds for a typical test flow condition of Mach number 0.7 and maximum Reynolds number of 40×10^6, based on a reference length of 0.1 m.

For a larger height of the test section, during the measuring time part of the shock tube boundary layer enters the test section and flows along the upper and lower walls. The maximum possible distance between these walls is to 280 mm. Increasing the height of the test section results in smaller blockage ratios, with the advantage of reduced wall interference effects and increased Mach number capability. Experiments performed so far with different heights of the test section show, however, that the influence of the shock tube boundary layer inside of the test section is negligible on the flow around the model. The test section side walls are fixed at a position of 200 mm, which corresponds to the smallest possible distance of the lower and upper wall, that is, most of the shock tube boundary layer is peeled off at the side walls.

The test section is designed for a maximum static pressure of 4 MPa, which is necessary to achieve high Reynolds numbers on the order of 40×10^6 based on a model chord length of 100 mm. Between the test section and dump tank, another diaphragm may be installed to allow evacuation of the dump tank before testing. During the run, the gas expands into the dump tank. This leads to an expansion wave traveling upstream into the test section, which reduces the maximum achievable theoretical test time. Current experiments make use of a slightly convergent–divergent two-dimensional nozzle at the downstream end of the test section, which is not shown in Fig. 2. In the divergent part of the nozzle, the flow is accelerated to low supersonic speed. In this case, the expansion wave mentioned before as well as other disturbances are kept from traveling upstream into the test section.

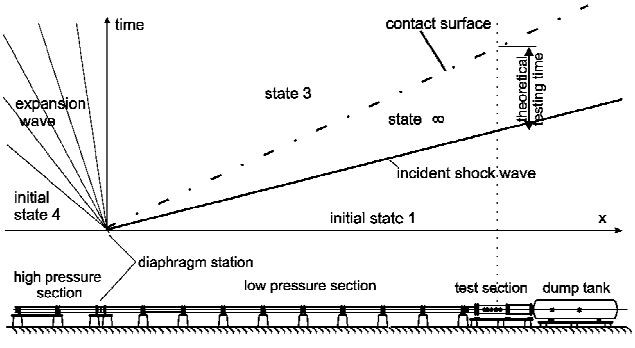

Fig. 1 Transonic shock tube and wave plan.

Calibration Experiments

The relatively small dimensions of the airfoil models with a maximum chord length of 100 mm and a maximum thickness of 11 mm prevent the direct installation of a high number of pressure transducers into the models. Furthermore, for high-Reynolds-number experiments, the aerodynamic loads lead to stresses in the model that are on the order of the strength of the model material. In this case, model or mounting failure should not lead to the loss of all transducers. Therefore, the pressure transducers, one for each pressure tap, are mounted in the inner side walls of the test section. They are connected to the surface pressure taps by thin pressure tubings about 150 mm long. The dynamic behavior of the complete pressure measurement system was investigated thoroughly, including pressure tap, tubing, pressure transducer, and data acquisition system. Length and inner diameter of the tubings were varied over a wide range. Figure 3 shows the response of five different pressure tubings to the pressure jump generated in a shock tube. All pressure taps were located in the same cross section. It is observed that the shorter is the tubing, the higher is the overshoot of the pressure signal, which is caused by oscillations of the gas column in the tubing. When the inner diameter of the tubing is reduced, damping caused by wall friction becomes more important. This leads to a reduction of the oscillation phenomenon but at the expense of a longer rise time. These counteracting effects necessitate the choise of an optimum inner tubing diameter for the pressure range considered. It is seen in Fig. 3 that, after nearly 5 ms, all tubings result in the same

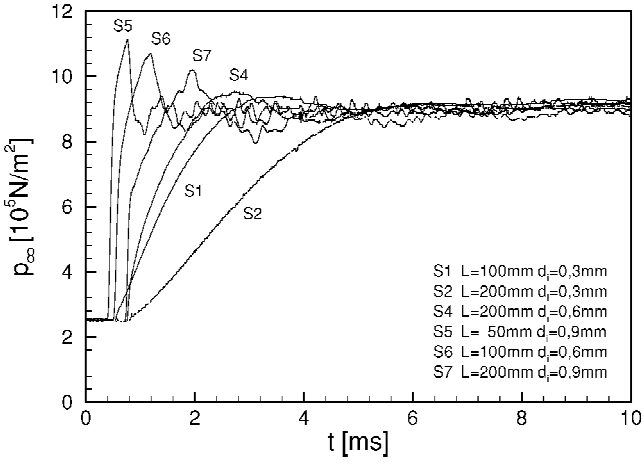

Fig. 3 Influence of diameter and length of pressure tubings on temporal signal behavior for a steplike pressure pulse.

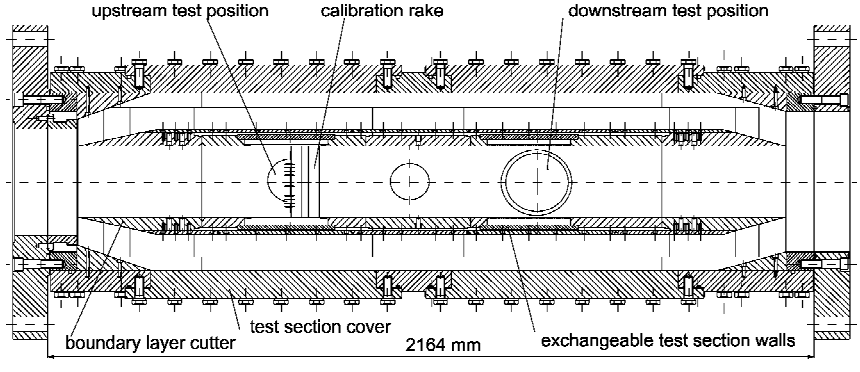

Fig. 2 Longitudinal section of the test section.

stationary pressure value within the experimental uncertainty. The remaining scatter of the signals during the stationary phase may be regarded as typical uncertainty of the pressure measurement, which is determined from Fig. 3 to be ±3%. These preliminary investigations gave evidence that, with a suitable pressure tubing of 150 mm length, pressure measurements at least for quasi-stationary flows are possible, provided the overall measuring time exceeds 3–5 ms. This is the case for the facility described in this paper.

The homogeneity of the test section flow was checked with a pitot rake, schematically shown in Fig. 2. The pitot rake, consisting of 15 pressure measuring locations, made use of the pressure tubings investigated in Fig. 3. The static wall pressure was measured in parallel, so that the freestream Mach number can be deduced from the pitot and static pressure. Figure 4 shows a typical example of a pitot and static pressure history. It is seen that during the useful running

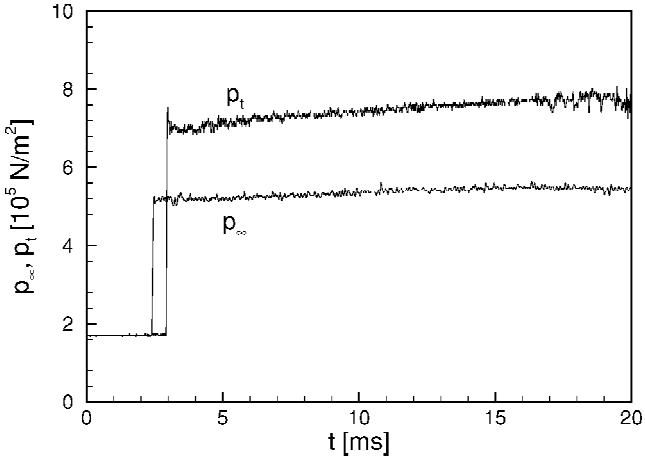

Fig. 4 Example of pitot and static wall pressure histories measured in the test section of the transonic shock tube.

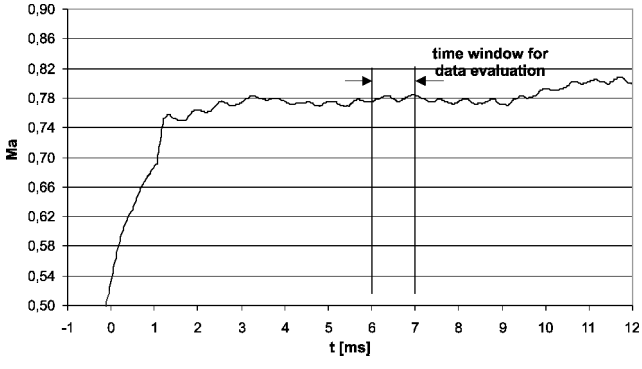

a)

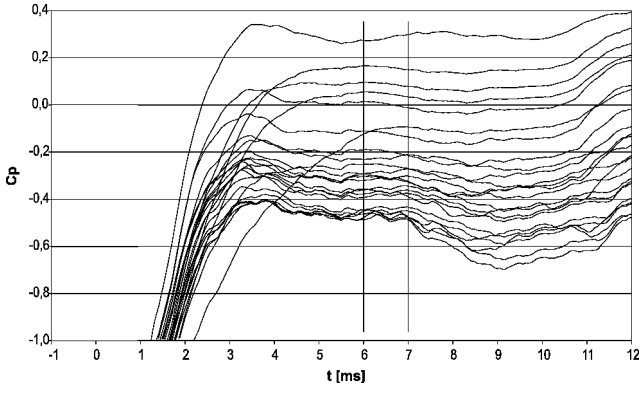

b)

Fig. 5 Typical time histories of Mach number and pressure coefficients along the upper side of an airfoil model; $Re = 38 \times 10^6$, reference length 0.1 m.

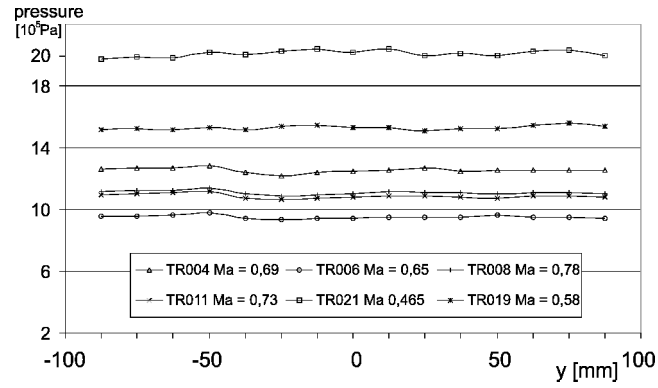

Fig. 6 Pitot surveys in the horizontal plane of the test section for different flow Mach numbers.

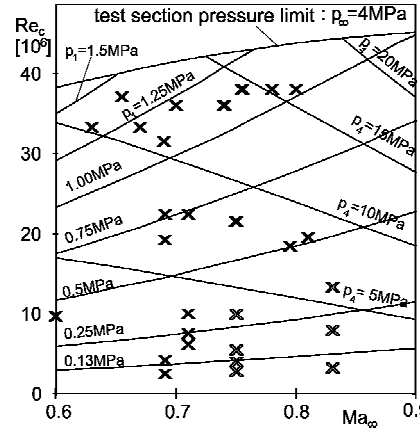

Fig. 7 Mach–Reynolds number envelope; reference length $l = 100$ mm.

time from 5 to 15 ms the pitot pressure as well as the static pressure rise slightly. Because the pitot pressure increases a little more than the static pressure, the freestream Mach number increases slightly with time. This effect is caused by the shock tube boundary layer, which results in a slight attenuation of the incident shock. Because of this, during the running time, at a fixed position the freestream Mach number increases by about 2–5%. Fortunately, before the Mach number starts to rise, in general a short period of testing time with constant Mach number can be identified. At present, this time window is used for final data evaluation. An example of this is given in Fig. 5, which shows the Mach number history and the histories of pressure coefficients for different positions along the upper side of an airfoil model described in the following section. In this case, the Mach number starts to rise at about 9 ms. Further research is related to shock tube methods, which results in an even more stationary flow behavior, as shown in Fig. 5. Furthermore, numerical studies have to be performed to prove the quasi-stationary flow behavior for time periods taking place after that indicated in Fig. 5. In this case, data reduction can be extended to longer running times than those given in Fig. 5. The pitot rake measurements revealed a spatially homogeneous flow in the test section. Figure 6 shows pitot surveys for the horizontal plane of the test section for various flow Mach numbers. The largest spatial deviation is 5%, which represents a typical value for shock tube facilities. Further effort devoted to an optimized design of the test section and to the measurement technique would lead to a reduced scatter and a more homogeneous flow. In Fig. 7, the Reynolds–Mach number envelope of the facility is shown together with calibrated conditions and experiments performed so far indicated by the cross symbols.

Results

A time-resolved shadowgraph system is set up for flow visualization, which allows 24 single frames per shot. In the following, only one representative frame for each experiment is shown. The airfoil model is fixed by two thin side plates with a thickness of 4.5 mm

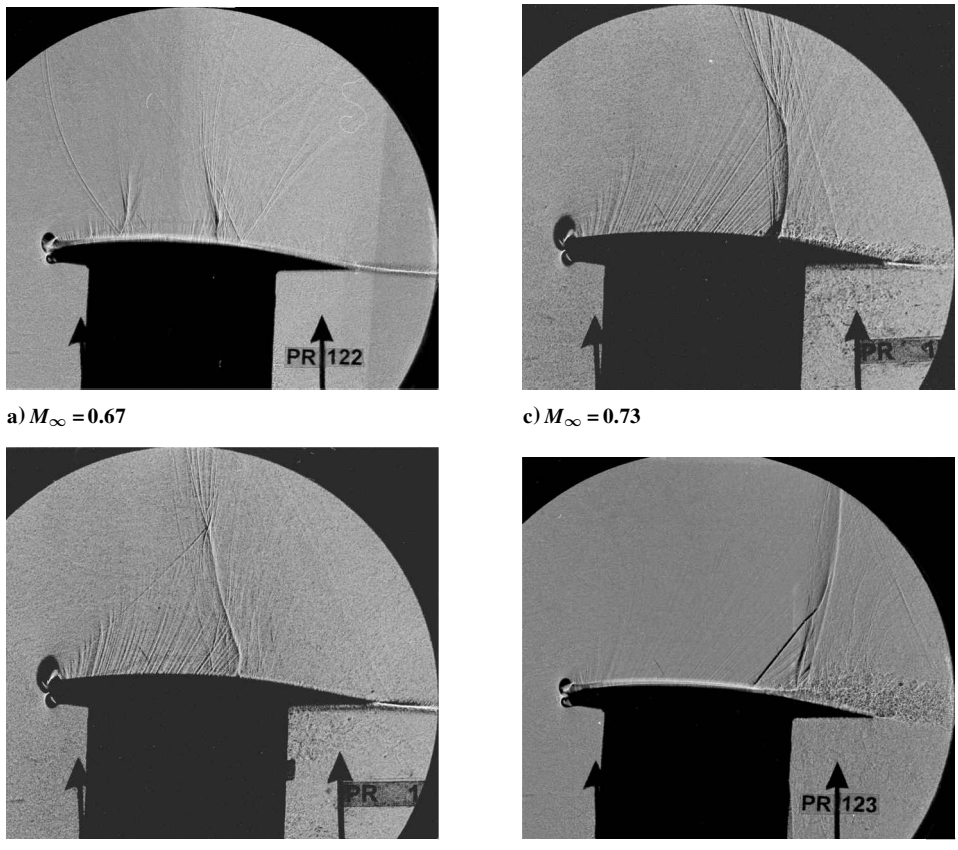

a) $M_\infty = 0.67$ c) $M_\infty = 0.73$

b) $M_\infty = 0.71$ d) $M_\infty = 0.77$

Fig. 8 Flow on the upper side of the airfoil BAC3-11; $\alpha = 2$ deg and $Re_c = 3.2 \times 10^6$.

for flow visualization. These plates are fixed at the two tunnel side walls. Therefore, either the upper or lower part of the airfoil and the corresponding flowfield is visible. Because of the high mechanical loading caused by the high-Reynolds-numberflow, the airfoil model cannot be fixed by clamping between the tunnel windows.

In Fig. 8, the influence of the freestream Mach number is exemplarily shown for an angle of attack of 2 deg. For the low-Mach-number case (Fig. 8a), a weak two-shock system develops. Because of the off-axis arrangement of the 24 sparks and receiving optics, a small vertical shift of the picture occurs, which is especially visible along the upper surface of the airfoil in Figs. 8a and 8d. With increasing Mach number, the two-shock system vanishes, and a single shock develops (Fig. 8b). The Mach lines in the supersonic region between the nose and shock are clearly visible, as well as the expansion region around the nose. The shock is still too weak to cause boundary-layer separation. For the slightly increased Mach number of 0.73, the shock becomes a little stronger, and as expected, its location is a little farther downstream. For this Mach number, a weak boundary-layer separation behind the shock takes place. For the highest Mach number considered (Fig. 8d), a strong separation is visible behind the shock. Furthermore, a lambda shock configuration develops, and the whole shock system moves farther downstream. In Fig. 8d, the Mach lines in the supersonic region are not as clearly visible as in the earlier case because of reduced sensitivity of the optical setup.

In addition to flow visualization, measurements of the pressure distribution around the airfoil have been performed. For this, a model of 200-mm span and 100-mm chord length has been built, with 24 pressure taps located on the upper side and 19 on the lower side of the model. As already mentioned, the relatively short running times of the facility do not allow for very small inner diameters of the pressure taps and very long connecting tubes to the pressure transducers. Based on the experimental results already discussed, the inner diameter of the pressure taps was chosen to be 0.6 mm and the typical length of the pressure tubing of each pressure tap to be 152 mm. The pressure taps are located in the midspan area of the model. Commercial piezoresistive pressure gauges have been used as pressure transducers.

In Fig. 9, some of the measured pressure histories are given for an experiment with a medium Reynolds number of 7.2×10^6 and a freestream Mach number of 0.74. In this case, a strong shock develops, especially on the upper side, which is visible in the shadowgraphs, as well as in the pressure distribution and time-resolved pressure histories. Along the upper side of the airfoil from the nose up to the position of $x/c = 52.3\%$, the pressure histories exhibit steady behavior after the flow establishment (Fig. 9). Downstream of this position, a shock develops during the flow establishment, which then moves downstream to stabilize its position at about $x/c = 67\%$. This development and the downstream movement are clearly visible for the pressure history at $x/c = 65.5\%$. After the shock has passed this position, the pressure becomes steady at a lower level. At its final position, the shock oscillates with small spatial amplitude, which causes the pressure fluctuations at $x/c = 68.5\%$. Farther downstream of the shock position, the pressure histories become more steady. A much weaker shock is generated on the lower surface, which causes slight pressure fluctuations at the position $x/c = 43\%$.

For this flow condition, shadowgraphs were taken separately for the upper and lower sides of the airfoil in two shots. They were put together to visualize the whole flowfield (Fig. 10). At the lower side, downstream of the nose, a first shock is generated at about $x/c = 5$–8%. This shock of small lateral extent is visible at the end of the dark region at the nose (Fig. 10). Behind this shock, the flow is subsonic, and consequently, no Mach lines are visible. However, the flow accelerates again to supersonic speed. In a high-quality copy, the supersonic region is clearly visible by the Mach lines. The end of this region is determined by the second shock at the lower surface.

The most interesting feature of the facility is the achievement of high-Reynolds-number flow. To now, the maximum Reynolds

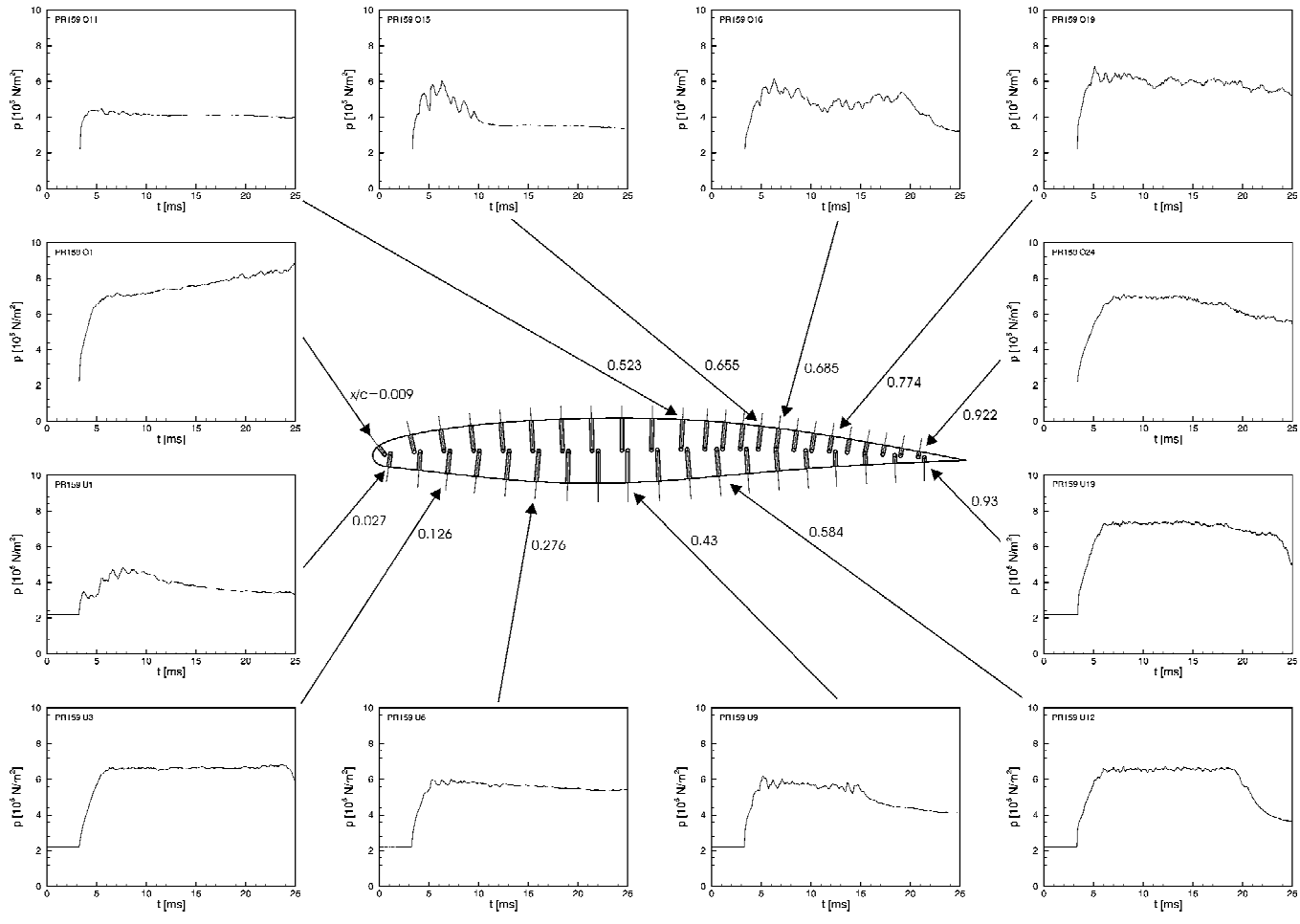

Fig. 9 Pressure histories for $M_\infty = 0.74$, $Re_c = 7.2 \times 10^6$, and $\alpha = 0$ deg.

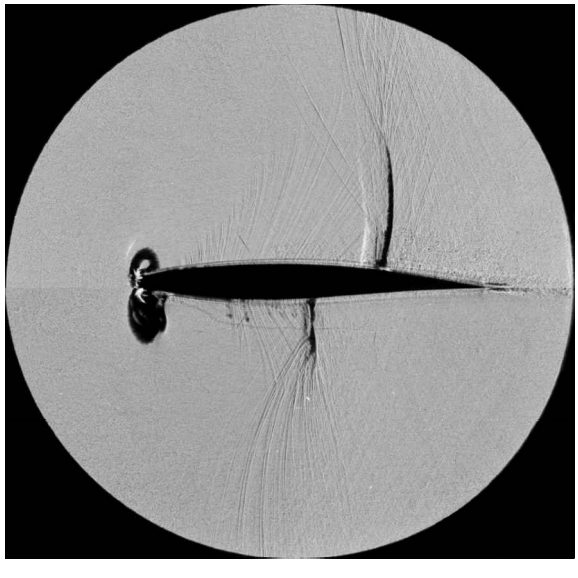

Fig. 10 Shadowgraph from two experiments, lower and upper sides; $M_\infty = 0.74$ and $Re_c = 7.2 \times 10^6$.

number based on the model chord length has been 38×10^6 for a Mach number of 0.8. Figure 11 shows pressure histories obtained for the upper and lower sides of the airfoil at an angle of attack of 0 deg for a medium Reynolds number of 20.5×10^6 and a Mach number of 0.7. On the upper side from $x/c = 47$ up to 65%, pressure fluctuations are visible in the signals caused by compression waves, which steepen to form a weak shock. For other positions during the measuring time, the pressure histories exhibit quite steady behavior. In the transonic shock tunnel, high Reynolds numbers are achieved by high static pressures. Therefore, in the pressure plots shown in Fig. 11, the maximum pressure on the airfoil model reaches up to 2.1 MPa, which represents a remarkably high value.

At $\alpha = 0$ deg for the low- and high-Reynolds-number cases, no significant difference can be detected on the shadowgraphs (Fig. 12). For the high-Reynolds-number flow, the expansion region around the nose is resolved in more detail, and the generation of a weak shock on the upper side becomes apparent. This weak shock or strong compression waves are responsible for the pressure fluctuations observed on the upper side of the airfoil in Fig. 11.

The Reynolds number influence becomes more pronounced for higher angles of attack, where a stronger shock develops. The interaction of the turbulent boundary layer with the shock for this special airfoil leads to a shock oscillation. The high temporal resolution capability of the measuring technique employed in these experiments allowed the study of these effects. Figure 13 gives the distributions of the pressure coefficient for 0- and 2-deg angles of attack for a low- (square symbols) and a high-Reynolds-number flow (circles) for three different times during the running time.[15]

The experiments at $\alpha = 0$ deg reveal an interesting phenomenon. If the flow approaches or slightly exceeds the critical state, that is, if the flow becomes sonic, it tends to exhibit unsteady behavior. This is visible for the pressure distributions on the upper side between $x/c = 35$ and 60%. The value c_p^* in Fig. 13 gives the pressure coefficient for which sonic velocity is reached. The development of a local unsteady flowfield is more pronounced for the high-Reynolds-number flow than for the lower Reynolds number. Upstream and downstream of this region the pressure coefficient shows a much more steady behavior. The situation changes if there is a strong shock imbedded in the flowfield, as in the case in Fig. 13b for 2-deg angle of attack. For the low-Reynolds-number flow during the time period between 7.5 and 9.5 ms, the shock moves a little downstream

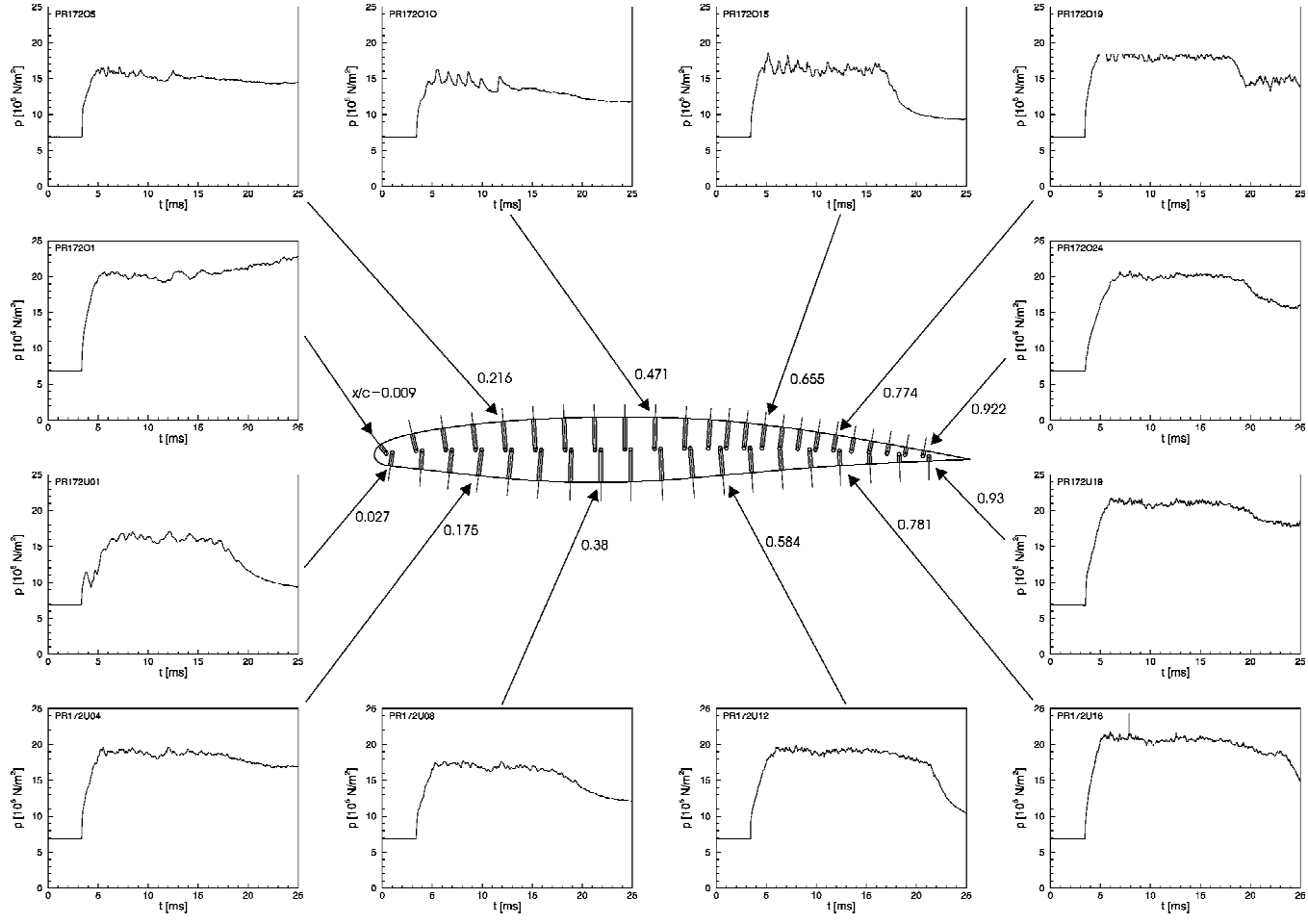

Fig. 11 Pressure histories for airfoil BAC3-11, $M_\infty = 0.7$, $\alpha = 0$ deg, and $Re_c = 20.5 \times 10^6$.

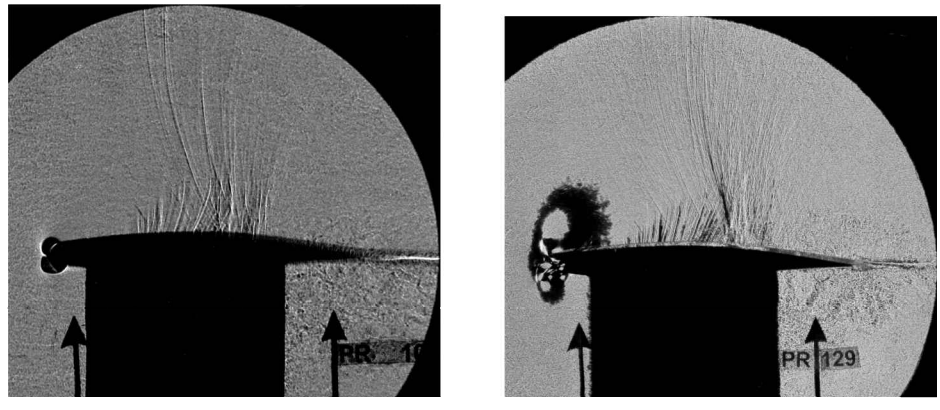

a) $Re_c = 3.1 \times 10^6$ **b) $Re_c = 20.7 \times 10^6$**

Fig. 12 Influence of Reynolds number on airfoil flow; $M_\infty = 0.71$ and $\alpha = 0$ deg.

very slowly. The velocity of this shock movement amounts to only 2 m/s, which is a relatively small value compared to the freestream velocity of 290 m/s, that is, there should be enough time to establish a quasi-steady flow during the shock movement. For the high-Reynolds-number case, the shock moves first upstream from about $x/c = 60$ to 56%. Then it moves downstream, and during the remaining measuring time, it becomes stationary at a position of about 60%. In this case, the shock position is located more upstream than for the low-Reynolds-number flow. Also the high Reynolds number leads to a lower suction pressure on the upper side but to a higher pressure on the lower side. Integration of the pressure distributions show that, despite the different distributions for this Mach number, the overall lift is practically not affected by the Reynolds number.

In Fig. 14, the pressure coefficient distributions are compared for an experiment with Reynolds number $Re = 20 \times 10^6$ with an experiment yielding a Reynolds number of $Re = 36 \times 10^6$ and for 0-deg angle of attack. The latter represents a test for almost maximum operating performance of the facility. In both cases, the Mach number of the freestream was 0.73, and as in all tests, there was no boundary-layer tripping. Furthermore, the pressure distributions are not corrected with regard to wall interference effects. This may also be of influence on the slightly higher pressure coefficients for

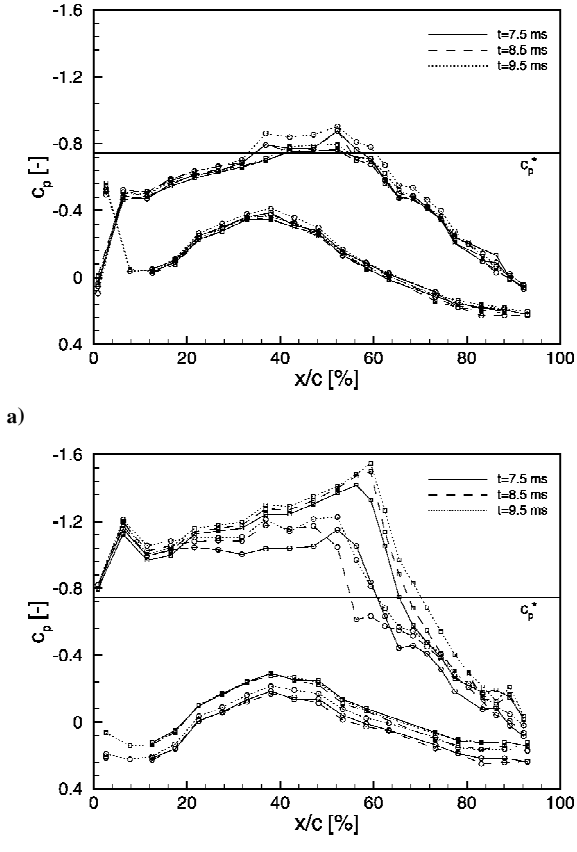

Fig. 13 Distribution of pressure coefficient, $M_\infty = 0.7$: a) $\alpha = 0$ deg: □, $Re_c = 2.7 \times 10^6$ and ○, $Re_c = 20.5 \times 10^6$; and b) $\alpha = 2$ deg: □, $Re_c = 7.5 \times 10^6$ and ○, $Re_c = 20.3 \times 10^6$.

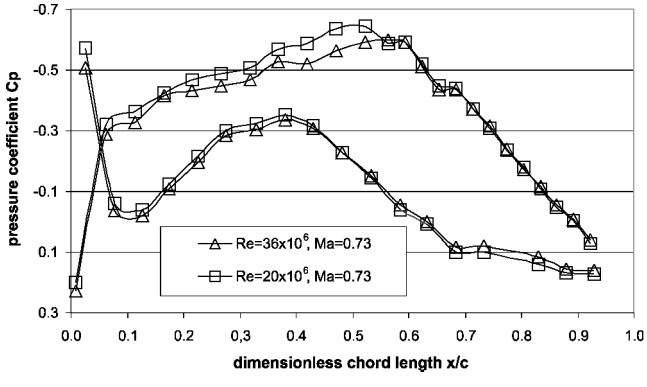

Fig. 14 Comparison of pressure coefficient distributions for airfoil BAC3-11 for two different Reynolds numbers; angle of attack $\alpha = 0$ deg.

the high-Reynolds-numbercase. Because in this case the boundary layer on the tunnel walls, as well as on the model, is thinner than for the lower Reynolds number, there is less of a blockage effect. In this case, the effective flow Mach number is lower than the nominal one, which yields slightly larger pressure coefficients, as for the smaller Reynolds number. On the upper surface of the airfoil, compression waves occur, which cause the pressure rise in the region from $x/c = 0.6$ to 0.7. These pressure waves are also visible on the shadowgraphs of Fig. 12. Obviously, the influence of the Reynolds number on the pressure coefficient is much less intensive for the recompression zone of the airfoil than for the accelerating part of the flow.

Conclusions

A shock tube has been rebuilt and used for airfoil testing in the transonic regime. The flow behind the incident shock is used as test flow. The airfoil models are installed in a rectangular test section that is located at the downstream end of the low-pressure section. The span of the models installed between the two tunnel side walls is 200 mm, whereas the height of the test section can be varied from 200 to 280 mm. The upper and lower test section walls can be equipped with slotted inserts to reduce wall interference effects. Experiments have been performed so far with airfoil models of 80- and 100-mm chord length. Time-resolved shadowgraphs show details of the flowfield, such as Mach lines, shocks, separation, etc. For pressure measurements, one model was equipped with 43 piezoresistive pressure transducers. The highest Reynolds number achieved so far is $Re_c = 38 \times 10^6$ based on 100-mm model chord length. The typical running time is on the order of 10–15 ms. Experimental results show that this time is sufficient for flow establishment and a quasi-steady flow period during which representative pressure coefficients and other data are determined. As is typical for transonic flow, the flow behavior strongly depends on the Mach number, which, therefore, needs a careful technique for determination. In this work, the Mach number has been determined from time-resolved pitot and static pressure measurements. These revealed that, due to the shock tube boundary-layer influence, the Mach number rises slightly with time. Up to now, representative quantitative data have only been taken during a short period of time during the running time, for which the Mach number is constant within the experimental uncertainty. Future work will be related to the study of different shock tube techniques that allow the time period of steady-state conditions to be prolonged. The pressure histories measured around the airfoil exhibit no unusual behavior. The fast measuring technique allows the detection of highly transient flow processes, such as pressure oscillations caused by shock oscillations, etc., which cannot be resolved with standard wind-tunnel measuring techniques. The results achieved so far show that with this type of facility very high Reynolds numbers that approach flight Reynolds numbers can be achieved easily and cost effectively.

Acknowledgments

This work has been funded by the Deutsche Forschungsgemeinschaft as part of the Collaborative Research Center SFB 401 "Flow Modulation and Fluid–Structure Interaction at Airplane Wings" at the RWTH Aachen University, Germany.

References

[1]Geiger, S. W., Mautz, C. N., and Hollyer, R. N., "The Shock Tube as an Instrument for the Investigation of Transonic and Supersonic Flow Patterns," Engineering Research Inst., Project M720-4, University of Michigan, Ann Arbor, MI, June 1949.

[2]Varwig, R. L., and Rosemann, L.,"A Seven Foot Diameter Shock Tube for Transonic and Supersonic Aerodynamic Testing," *Proceedings of the 5th International Shock Tube Symposium*, U.S. Naval Ordnance Lab., White Oak, MD, 1965, pp. 1091–1110.

[3]Cook, W. J., Presley, L. L., and Chapman, G. T., "Use of Shock Tubes in High Reynolds Number Transonic Testing," *Modern Developments in Shock Tube Research*, edited by G. Kamimoto, Proceedings of the 10th International Shock Tube Symposium, Shock Tube Research Society, Kyoto Univ., Kyoto, Japan, 1975, pp. 472–479.

[4]Cook, W. J., "A Study of Test Section Configuration for Shock Tube Testing of Transonic Airfoils," NASA Ames Research Center, Final Rept., Grant NSG-2152, 1978.

[5]Cook, W. J., Chaney, M. J., Presley, L. L., and Chapman, G. T., "Application of Shock Tubes to Transonic Airfoil Testing at High Reynolds Numbers," NASA TP 1268, 1978.

[6]Cook, W. J., Presley, L. L., and Chapman, G. T., "Shock Tube as a Device for Testing Transonic Airfoils at High Reynolds Numbers," *AIAA Journal*, Vol. 17, No. 7, 1979, pp. 714–721.

[7]Cook, W. J., Presley, L. L., and Chapman, G. T., "Use of Shock Tubes in High Reynolds Number Transonic Testing," *Shock Tubes and Waves*, edited by A. Lifshitz and J. Rom, Proceedings of the 12th International Symposium on Shock Tubes and Waves, Hebrew Univ., Jerusalem, 1980, pp. 127–136.

[8]Cook, W. J., and Heidegger, N. J., "Dense Gas Aerodynamic Studies in a Shock Tube," NASA Ames Research Center, Progress Rept., Contract NAG 2-175, 1993.

[9]Yamaguchi, Y., "Performance of a Slotted Wall Test Section for Aerodynamic Testing in a Shock Tube," *Theoretical and Applied Mechanics*, Vol. 37, 1989, pp. 39–47.

[10]Yamaguchi, Y., and Amemiya, T., "A Preliminary Study on the Fixed Transition Technique for a Shock Tube Transonic Airfoil Flow," *Transactions of the Japan Society for Aeronautical and Space Sciences*, Vol. 37, No. 118, 1995, pp. 311–318.

[11]Yamaguchi, Y., Amemiya, T., and Wada, S., "Application to Trip Strips of Shock Tube Airfoil Flows," *Shock Waves*, edited by R. R. Boyce, P. M. Danehy, M. Hannemann, J. J. Kurtz, T. J. Mclntyre, S. J. McMahan, D. J. Mee, R. J. Sandeman, and H. Tanno, Panther Publishing and Printing, Canberra, Australia, 1997, pp. 529–534.

[12]Yamaguchi, Y., Kaibara, K., and Saito, T., "Application of Wall Interference Corrections to a Low Aspect Ratio Airfoil Model," AIAA Paper 97-0916, Jan. 1997.

[13]Reichel, T., Zechner, M., and Olivier, H., "Der Stoßrohr-Transschallkanal der RWTH Aachen, ein 2-D Windkanal zur gleichzeitigen Einhaltung von Mach- und Reynoldszahlähnlichkeit," *DGLR Jahrestagung*, Paper DGLR-JT2000-017 [CD-ROM], Sept. 2000.

[14]Mirels, H., "Shock Tube Test Time Limitation due to Turbulent-Wall Boundary Layer," *AIAA Journal*, Vol. 2, No. 1, 1964, pp. 84–93.

[15]Zechner, M., "Transsonische Profilumströmungen im Stoßrohr-Transschallkanal," Ph.D. Dissertation, Shock Wave Lab., Aachen Univ., Aachen, Germany, April 2002.

G. V. Candler
Associate Editor